Pharm Res (2012) 29:2792–2805
DOI 10.1007/s11095-012-0717-5

RESEARCH PAPER

A Practical Method to Predict Physical Stability of Amorphous Solid Dispersions

Stéphanie Greco • Jean-René Authelin • Caroline Leveder • Audrey Segalini

Received: 31 October 2011 / Accepted: 20 February 2012 / Published online: 16 March 2012

ABSTRACT

Purpose To predict the crystallization time of amorphous solid dispersions by controlling the combined effect of temperature and moisture content.

Methods The authors exposed amorphous samples of spray-dried API and Hydroxypropylmethylcellulose Phtalate to various temperature and humidity conditions below and above the glass transition temperature (Tg) until crystallization of the API was observed. The crystallization of API was detected by XRPD, while the T_g and the water absorption by the amorphous dispersion are quantified by mDSC and water sorption analysis.

Results Extrapolation of the data obtained at a temperature above T_g to conditions below T_g gives only a qualitative trend. By contrast, in conditions below T_g the logarithm of onset of crystallization time was shown to vary linearly with the T_g/T ratio. A statistical analysis shows that the data obtained in the highest temperature/humidity conditions, for which the onset of crystallization is below 3 months, can be extrapolated over 15 months.

Conclusions The proposed methodology can be used as a stress program to predict long-term stability from a relatively short observation period and to design appropriate temperature and humidity conditions for long-term storage to prevent crystallization.

KEY WORDS amorphous · crystallization onset · glass transition temperature · moisture · physical stability

S. Greco (✉) • J.-R. Authelin • C. Leveder • A. Segalini
Sanofi
Vitry-sur-Seine, France
e-mail: Stephanie.greco@sanofi-aventis.com

INTRODUCTION

The proportion of drugs exhibiting a poor bioavailability due to their poor water solubility has significantly increased in the last years (1). One of the most successful ways to solve this problem is to improve the drug release of such pharmaceutical solids by developing an amorphous form, generally as a solid dispersion with polymeric carriers (2–5). The high energy state of the amorphous form confers to it higher solubility and enhanced bioavailability through improved dissolution. Consequently, the use of amorphous phases has been the subject of very intensive investigations in the pharmaceutical field (6–11).

One of the main challenges of these solid amorphous forms is the physical instability associated with the high energy state, and the difficulty to forecast potential instability. How can one predict rapidly, during the evaluation of different candidate formulations, the long term stability (for instance over 2 years) of these metastable products? The extrapolation of accelerated conditions, classically used for chemical degradation (ICH Q1E guideline)-which claims that data for 6 months at 40°C 75%RH is predictive for 24 months at 25°C/60% RH- cannot be applied here. Hence real time stability studies, both time-consuming and costly, are necessary to anticipate physical stability. The aim of this article is to propose a methodology that would enable the prediction of long term physical stability from appropriate accelerated studies.

Our objective is hence very practical, but in order to attain it, this study must be based on the theoretical equations describing the mechanisms which underlie the instability of amorphous systems. Numerous publications have shown that the molecular mobility of the amorphous phase is responsible for chemical (6,12) and physical instabilities (9,13–17). It is commonly known that the molecular

mobility of an amorphous compound is due to two main relaxations (18,19), called α- and β- relaxations. The β-relaxations are linked to local molecular movements and have an Arrhenius behaviour over the whole range of temperature. The α-relaxations are linked to cooperative molecular motion. For these movements, the temperature dependence of the relaxation time is described by the Adam Gibbs model, with three different regimes, described in Fig. 1. Above T_c (Cross over temperature where α and β relaxation times are similar), the α -relaxation time follows Arrhenius behaviour. For temperatures Between T_c and T_g, the α relaxation time exhibits a non linear temperature behavior that follows the Vogel-Tammann-Fulcher (VTF) law (see theoretical interpretation part). Finally below T_g, the molecular structure of the amorphous phase is frozen and the relaxation time behaves again according to the Arrhenius law (18).

Among the numerous attempts to correlate molecular mobility of the amorphous solids with physical instability, some work can be highlighted here. Alié and co-workers (14) attributed the crystallization rate of a pure amorphous drug to β relaxations in the temperature range above T_g, suggesting that molecular rearrangements were the rate limiting step. More frequently the crystallization times are attributed to α-relaxations, as diffusion seems to be the main limitation for the crystallization kinetics. Both cases may however exist depending on the molecular properties and the rate limiting step.

For phenobarbital, nifedipine and their dispersions with PVP, Aso and collaborators (17,20) demonstrated a strong correlation between the α-relaxation times, measured by DSC and solid state NMR, and the crystallization rates, above and below T_g. Bhugra and co-workers (13,21) evaluated the relaxation times of amorphous sucrose by dynamic relaxation spectroscopy, isothermal microcalorimetry and modulated DSC, and showed that above T_g a strong coupling exists between these measurements and the crystallization onset. They then used this correlation in order to predict "semi-quantitatively" the crystallization onset below T_g.

These studies evaluated the impact of the temperature, but another parameter also plays a very important role: the humidity. Indeed, the humidity is responsible for decreasing the T_g of amorphous solid samples due to the plasticizing effect of water, and consequently favors the crystallization phenomenon. Interestingly, Miyazaki *et al.* (22) showed how the humidity and the temperature can be coupled in a unique parameter, T_g/T. In the $T > T_g$ region, they found that the crystallization rate of amorphous nifedipine has an Arrhenius-like behaviour when expressed as a function of T_g/T. Similar results were obtained by Schmitt *et al.* (23) on spray dried amorphous lamotrigine mesylate. Indeed, when exposing the drug to moisture, a parallel decrease of T_g and crystallization onset was observed by DSC (hermetic pans). Based on their published data, we calculated that the ratio T_g/T_{onset} (in K) is approximately constant (0.84–0.87) (Table I). These data, represented in Fig. 2, suggest that temperature rescaling by T_g may reveal interesting properties considering physical stability.

As it has been demonstrated in the literature, it is possible to utilize the combined effect of temperature and humidity in order to simply correlate the crystallization kinetic with a unique parameter T_g/T. In this study, we propose to use this idea in order to extrapolate physical stability at a long time period from data obtained at low temperatures (≤60°C) and high humidities. For this purpose, we used a Sanofi drug substance called SAR. SAR is a very insoluble BCS class II compound, formulated as a spray dried amorphous solid dispersion in HPMCP (20% SAR/80% HPMCP w/w). We propose to expose this sample to different temperatures and humidities and to characterize the crystallization onset for different T_g/T values. For the long term sub T_g studies, we used the methodology developed by Miyazaki (22), which

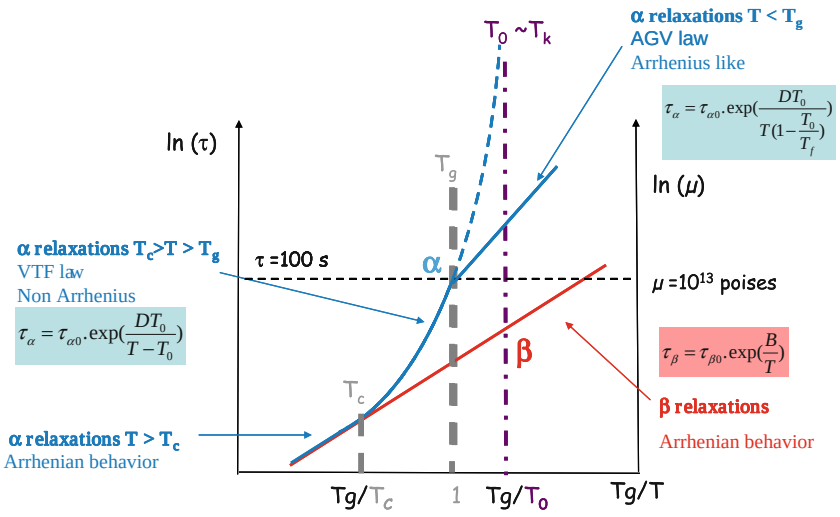

Fig. 1 α and β relaxation times represented as a function of T_g/T (adaptated from 18).

Table I T_g, Temperature of Onset of Crystallization for Lamotrigine Mesylate from Schmitt *et al.* (23) as a Function of Moisture Content - The T_g/T_{onset} Ration was Calculated by the Authors

Moisture%	T_g (°C)	T_{onset} crystallisation (°C)	T_g/T_{onset} (Kelvin values)
0.71	98.6	155.6	0.87
0.89	90.9	155.2	0.85
1.25	82.7	152.7	0.84
1.74	68.7	123.7	0.86
2.28	58.6	113.3	0.86
2.75	49.8	105	0.85
3.56	40.8	93.3	0.86
3.83	38.6	89.3	0.86
4.09	31.2	85.3	0.85

modulates T_g by exposing the product to various relative humidity values.

As has been reported by several authors (13,14,21), we characterize the crystallization by determining the onset of crystallization time "τ_{oc}". The detection of the crystallinity of the drug substance is a critical experimental point in this study. Indeed, from a practical point of view, it is the end of shelf life: until crystals are experimentally detected, the product will be considered as still amorphous and compliant. Nucleation however probably occurs slightly before. In numerous papers the crystallization rate was measured by DSC or by optical microscopy (24,25) for pure amorphous drugs or solid dispersions with a maximum of 20–25% of polymer (17,20,22,26). XRPD was used by Yoshioka *et al.* (27) to quantify precisely the degree of crystallinity of initial pure amorphous drug. Onset times of crystallization have been measured at $T > T_g$ either by DSC (13); or by dielectric spectroscopy isothermally (14). Onset times for $T < T_g$ have been measured by polarized microscopy (13) In this work, a simple and straightforward XRPD method was developed

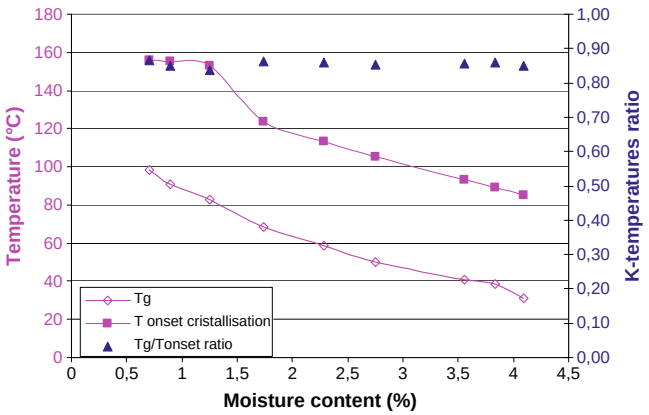

Fig. 2 Spray dried amorphous amorphous lamotrigine mesylate T_g, crystallization onset and T_g/T_{onset} ratio *vs.* moisture content adapted from Schmitt *et al.* (23).

to measure the crystallization onset for solid dispersions at low drug loads (20%).

The different steps of the present study are the following:

- To establish the impact of temperature and humidity on physical stability over a long time period (in the $T < T_g$ domain)
- To determine if long term (15 month) stability could be predicted on the basis of 3 month "stress condition" data (in the $T < T_g$ domain)
- To perform some measurements for $T > T_g$ in order to determine if there is a reasonable chance to predict sub T_g physical stability based on crystallization kinetics at $T > T_g$

MATERIALS AND METHODS

Materials

SAR is a drug compound developed by Sanofi-Aventis. HPMCP HP55 was supplied by Shin-Etsu Chemicals Co. (Tokyo, Japan). For the spray-drying process, EtOH and methylene chloride were purchased from Solvay (Brussels, Belgium). Silica gel and NaCl were obtained from VWR International, LLC (Radmon, Pennsylvania, USA). K_2SO_4, NaBr and $(NH_4)_2SO_4$ are purchased from Thermo Fisher Scientific Inc. (Waltman Massachusetts,USA).

Preparation of the Sample by Spray-Drying

SAR was dissolved with HPMCP HP55 in the solvent mixture CH_2Cl_2/EtOH 95%/5%. The ratio SAR/HPMCP was 20%/80% and the total solid concentration was 6.2% (all percentages are given in weight ratios). The final solution was atomized with a large pilot-scale loop spray-drier supplied by the Drytec company (diameter: 1 m, length: 3 m, gas flow approx. 500 kg/h). Inlet and outlet temperatures were fixed at 95°C and 50°C. A bifluid nozzle was used. After spray drying, the residual solvents (about 3%) were fully removed to well below ICH specifications by drying under vacuum (P~50 mbar).

Storage of Samples in Stressed Conditions for $T < T_g$

The measurements performed in the low temperature domain ($T < T_g$) represent the most important part of the experimental data of this study. The samples were conditioned at fixed temperature and humidities by placing them over saturated salt solutions at 60, 75, 80 and 100%RH, or over silica gel (0%RH) in closed glass desiccators either at room temperature (23°C) or in ovens at 40, 50, 55, 60 and 96°C. The storage conditions are summarized in Table II.

Table II Temperature and RH of Storage,Corresponding Salts Used To Control Humidity

Storage T (°C)	Storage RH (%)	Salt
96	0	Silical gel
60	80	$(NH_4)_2SO_4$
55	80	$(NH_4)_2SO_4$
50	100	K_2SO_4
50	80	$(NH_4)_2SO_4$
50	75	NaCl
40	100	K_2SO_4
40	80	$(NH_4)_2SO_4$
40	60	NaBr
23	100	K_2SO_4
23	80	$(NH_4)_2SO_4$
23	75	NaCl

The samples were removed and analyzed by XRPD at regular intervals of time. Analyses were carried out every 2 or 3 days for up to 20 days, followed by every week for 10 weeks, and then once every month for evaluations longer than 10 weeks. Except for one sample stored at 23°C and 100%RH, the analyses were discontinued upon crystallization of the sample.

For studies carried out in the high temperature domain ($T > T_g$), only the temperature was varied, the humidity being fixed to 0%RH for practical reasons (see the section on the T-XRPD analysis).

Modulated DSC

A MDSC Q200 supplied by TA Instruments (New Castle, Delaware USA) was used for T_g measurements. Samples from 2 to 10 mg were subjected to a modulated heating program from room temperature to 250°C, at a heating rate of 3°C/min, a period of 60s and amplitude of 1°C,. Depending on the requirements of the experiment (dry or humid conditions) hermetically or non-hermetically sealed pans were used. T_g was measured on the "reversing" heat flow signal, using the software Universal Analysis from TA Instruments. The T_g was calculated as the mid-point at the half height of the glass transition.

XRPD Analysis

A XRPD diffractometer, running at ambient temperature, was used to assess the crystallinity of the samples stored at fixed T and humidity conditions ($T < T_g$). Analyses were performed using a D8 Advance diffractometer from Bruker AXS (Madison, Wisconsin USA), with a Bragg-Brentano focusing geometry (θ-θ) in the reflection mode. The diffractometer is configurated with a LinxEye detector. A tube with an anticathode of copper running at 40 kV and 40 mA was used. Two lines are typically emitted: Cu$K\alpha$1 (λ=1.54060 Å) and Cu$K\alpha$2 (λ=1.54439 Å). The incident radiation was filtered to eliminate the K_β radiation. The parameters employed were as follows: scan range from 5 to 30 °2θ, with a step of 0.02° 2θ and 3 s of counting per step.

The onset time of crystallization (t_c) was defined by the appearance of more than one peak in the SAR diffractogram, that is, the time when the first SAR crystals are detected by XRPD. The limit of detection of crystallinity this method has been estimated to be 3% for SAR (unpublished data).

By convention, the crystallization onset (t_{oc}) was taken as the mean time between the last time where no crystallinity was detected (t_{nc}) and the first time where crystallinity was detected (t_c): $t_{oc} = (t_{nc} + t_c)/2$.

Variable T-XRPD Analysis

A XRPD diffractometer with a temperature chamber was used to assess the crystallinity of the samples exposed to temperatures above T_g, and 0%RH. Tests were carried out with a Bruker D5000 diffractometer equipped with the Bragg- Brentano parafocusing (θ-θ) geometry and an Anton-Paar TTK450 temperature chamber flushed by dry nitrogen. The powder was deposited in a concave stainless steel sample holder. A sealed cobalt anode X-ray tube running at 40 kV and 30 mA was used on this diffractometer. Two lines are typically emitted: Co$K\alpha$1 (λ=1.7890 Å) and Co$K\alpha$2 (λ=1.7929 Å). An Iron β-filter, placed between the detector and specimen, does not altogether eliminate Co$K\beta$ (λ=1.6208 Å) radiation, which still contributes about 1% of the diffracted beam at the detector (manufacturer's data). The beam is sighted using Soller slits, to improve its parallelism. Variable divergence slits keep the illumination area of the sample constant. A 1 mm collimator limits diffusion between the tube and the sample. A Braun 50-M multichannel linear detector completes the setup.

Temperature was allowed to increase at a rate of 0.05°C/sec. The following temperatures were used: 115, 116, 126 and 136°C. Diffractograms were recorded between 5 and 35° 2θ, with a step of 0.02° 2θ and 1 s of counting per step. The time of counting was reduced in comparison to standard XRPD, at room temperature, because the time of crystallization is very low for elevated temperatures (example: around 90 mn for 136°C) and rapid scans are hence necessary. Data were acquired in the isotherm mode when the requested temperature was reached.

Water Sorption Cycle

The sorption-desorption isotherms were recorded by a VTI SGA100 instrument. The SGA100 measures the uptake and loss of vapour gravimetrically using a Cahn D200 recording ultra-microbalance with a mass resolution of ±0.1 µg.

Controlled relative humidity was obtained by mixing dry gas and water saturated carrier gas streams (monitored by mass flow controllers), and measured continuously by a dew point controller. The temperature in the sample and the reference chambers was controlled to ±0.1°C by a water bath from Polyscience.

A sample size between 4 and 10 mg was used. Prior to being exposed to any water vapor, the samples were dried at 0%RH to remove any surface water present and to establish a dry, baseline mass. Next, the samples were exposed to four different relative humidity values: 20, 60, 75 and 80%RH. At each stage, the sample mass was allowed to reach equilibrium before the relative humidity was increased or decreased (the criterion for equilibrium was established when the weight variation did not exceed the value of 0,001 wt% during 5 min). If the equilibrium state was not reached after 1000 min, the relative humidity was changed to the next level automatically. The sorption isotherms were recorded at three different temperatures: 25, 40 and 50°C.

Statistical Methods for the Predictive Modelling

Analysis of data was performed using Enterprise Guide 4.3 with the SAS v9.2 software with PC Windows XP.

For the analysis, the crystallization onset t_{oc} is converted to log10.

Preliminary Descriptive Analysis

For each %RH storage condition of interest (except for 0%RH), a linear regression was performed.

Data Analysis

An Analysis of Covariance (ANCOVA) was used to test the whether the variances for the data from the different % RH storage conditions could be pooled.

- If the test for equality of the slopes resulted in a $p<0.25$, then each condition was treated separately.
- If the test for equality of the slopes resulted in a $p>0.25$ and the test for equality of the intercepts in a $p<0.25$, the calculations were done for each condition but the common slope was used.
- If the test for equality of the slopes and intercepts both resulted in a $p>0.25$, the data were pooled.
- Predictive model: A 95% predictive confidence interval was obtained for the crystallization onset for samples stored for less than 3 months. The residuals were checked to verify that they were randomly distributed around 0 and fell between −2 and 2. The 95% one-sided lower confidence is used in order to predict the worst case scenario.

RESULTS

Amorphous solid dispersions of SAR/HPMCP (20/80) obtained by spray-drying, were stressed at different temperatures and humidities (Table II) for several months. At defined intervals, samples were analyzed by XRPD at room temperature to evaluate the time of onset of SAR crystallization. The impact of humidity on the T_g of the amorphous dispersion is evaluated before discussing the correlation between the crystallization onset and T_g/T.

The Impact of Water Sorption on T_g

The first step was the determination of the water sorption by the amorphous material. In Fig. 3 the weight variation is plotted as a function of %RH for three temperatures (25, 40 and 50°C). Interestingly, the three isotherms are superimposable. This can be explained by the fact that the heat of water desorption from the solid is close to the heat of pure water evaporation. It is usually the case for the hydration of organic compounds as shown by Khankari *et al.* (28). Both the equilibrium vapour pressure above the solid at given moisture, and that of pure water have a nearly parallel evolution with temperature according to Van't Hoff's equation, and the sorption isotherm expressed as a function of the %RH is nearly temperature independent. We did not measure the sorption isotherm at 60°C, for practical reasons, but based on the previous discussion we assumed that it was not significantly different from those obtained at the other temperatures.

The T_g of the spray-dried samples was measured by mDSC (using hermetically sealed pans) after equilibration at each %RH and at room temperature (23°C). There was no deliquescence at 100% RH. An example of the mDSC reversing curve is presented in Fig. 4. We observed a single T_g independently of the sorbed water amount suggesting that the water does not result in amorphous phase separation. The T_g can then be represented as a function of the

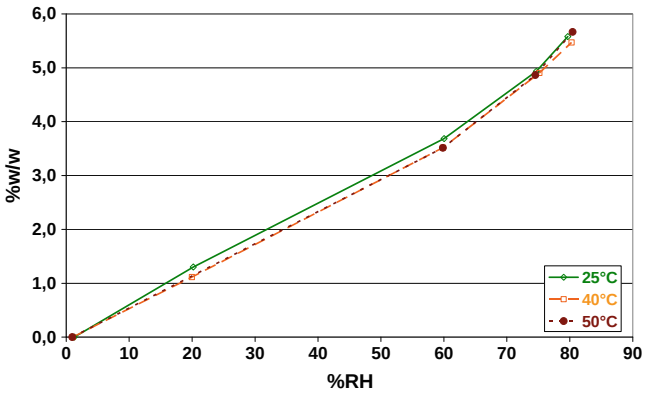

Fig. 3 Water sorption measured by VTI for the SAR/HPMCP sample as a function of RH% at the different storage temperatures: 25°C, 40°C and 50°C.

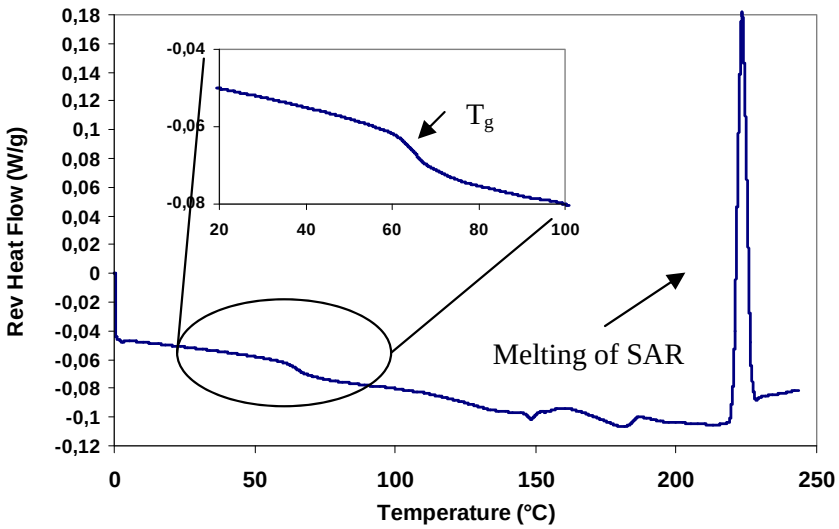

Fig. 4 mDSC "reversible" signal and T_g measurement for the SAR/HPMCP sample exposed to 80%RH, 23°C.

corresponding relative humidity. In Fig. 5, when the T_g of the solid disperstions is plotted as a function of the water content, a straight line is obtained which fits the theoretical Gordon-Taylor equation (Eq. 1) (29–31).

$$T_g^{GT} = \frac{w_{dry} T_g^{dry} + K w_{H_2O} T_g^{H_2O}}{w_{dry} + K w_{H_2O}} \quad (1)$$

where w_{dry} and w_{H_2O} are respectively the weight fraction of dry amorphous sample and of the adsorbed water on the total weight of the sample. T_g^{dry} is the T_g of the dried sample, and $T_g^{H_2O}$ the T_g of pure water (135 K). K is a constant that can be approximated by the Sihma Boyer rule (29–31):

$$K = \left(\rho_{dry}\ T_g^{dry}\right) \Big/ \left(\rho_{H_2O}\ T_g^{H_2O}\right) \quad (2)$$

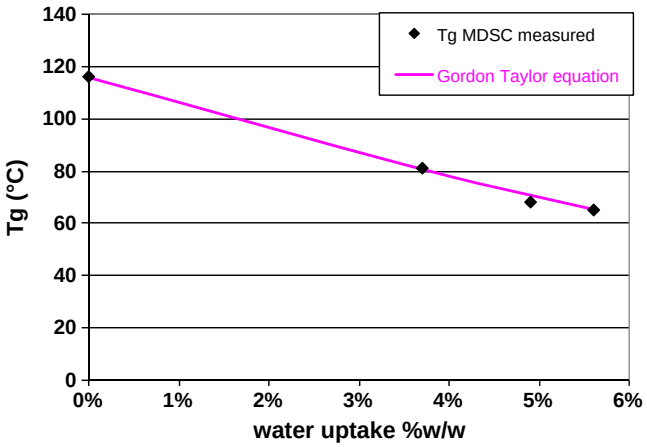

Fig. 5 T_g as a function of water uptake. The symbols plot the T_g measured by MDSC, and the solid line represents the theoretical T_g according to Gordon-Taylor relation.

where ρ_{dry} and ρ_{H_2O} are respectively the densities of the dry amorphous solid dispersion (estimated to be 1.31 g/cm^3) and of the amorphous ice (of 0.9 g/cm^3). The resulting value of K is 4.19.

The linear plot in Fig. 5 indicates that the plasticizing effect of water can be modelled by the Gordon Taylor equation.

Onset of Crystallization Time Measurements

Results for $T < T_g$

The onset of the SAR's crystallization was monitored by XRPD at regular intervals of time. As an example, Fig. 6 illustrates the evolution of the XRPD diagram of the SAR sample stored at 23°C and 100%RH, from 3 to 6 months. For this particular example the first time where crystallization was detected after storage was 120 days (t_c), and the last time where the sample was considered as purely amorphous was 90 days (t_{nc}). Thus for this example the crystallization onset t_{oc} is defined as 105 days.

For each humidity and temperature storage conditions, T_g/T, t_{nc}, t_c and t_{oc} measured values are presented in Table III. The measurements for samples stored at 50°C and 75%RH were repeated twice, to test the reproducibility of this method. For practical reasons the stability study was limited to 17 months, and consequently the T_g/T values studied here do not exceed 1.15. In the following chapters we propose to extend the observed correlation law above this value, but we are aware that this assumption is not verified here.

Results for $T \geq T_g$

These analyses were performed directly in the temperature chamber of the X-ray powder diffractometer. The relative

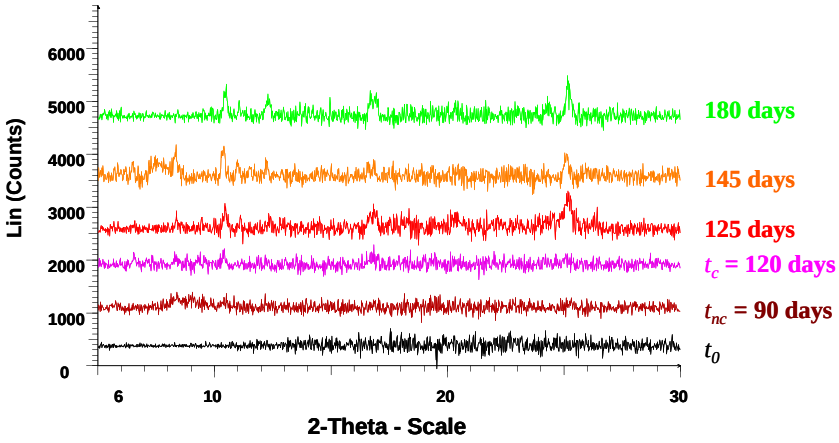

Fig. 6 XRPD diagrams of the solid dispersion SAR/HPMCP stored at 23°C and 100%RH, at different times.

humidity was maintained at 0%RH by a nitrogen flow and the temperature was precisely monitored. The sample was left in the chamber at a fixed temperature above the T_g value (116°C) for several hours until crystallization occurred. As an example, some of the XRPD diagrams recorded at 126°C are shown in Fig. 7. These four diffractograms correspond to the following successive times of exposure: the initial time t0, the exposure time of 6.3 h corresponding to t_{nc}, the 7.4 h point corresponding to t_c, and the final time. From this data, the onset of crystallization at 126°C is about 6.8 h. All crystallization times are summarized in Table IV.

Correlation between T_g/T and t_{oc}

In Fig. 8 the crystallization time is plotted as a function of $1000/T$ in an Arrhenius plot for various %RH conditions. The vertical error bars are taken as the maximal uncertainty on the crystallization time measurements for each domain, $T < T_g$ and $T > T_g$. The horizontal error bars correspond to the uncertainty in temperature, of about 2°C for low temperature region ($T < T_g$), and 0,5°C for high temperature region. It was estimated by comparing the set point of the oven regulation, or of the XRPD chamber, with local temperature measurements using calibrated probes. Figure 8 shows that in the low temperature domain $T < T_g$, the points are aligned on a different line for each humidity condition.

In Fig. 9, t_{oc} is plotted as a function of the rescaled reverse temperature T_g/T. The principal observations drawn from Fig. 9 are the following:

- There is a significant slope change around $T_g/T=1$, showing dramatically different behaviours on both sides of the T_g, as expected for α-relaxation driven mechanisms.
- At $T < T_g$ all crystallization onsets are well aligned *versus* T_g/T in the half logarithmic plot. The agreement is very good for the observation period of 17 months. This graph shows that the impact of both parameters,

Table III Crystallization Onset Measurements for all the Samples Stored in Desiccators (at Controlled T and %RH) for T Inferiors to T_g

Storage T (°C)	Storage RH (%)	%w/ w water	T_g (°C)	T_g/T	t_{nc} (days)	t_c (days)	t_{oc} (days)	uncertainty%**
96	0	0%	116	1.054	30	34	32	6
60	80	5.6%	65	1.015	10	12	11	9
55	80	5.6%	65	1.031	16	19	17.5	9
50	100	nd	53	1.009	13	14	13.5	4
50	80	5.6%	65	1.046	25	31	28	11
50	75	4.9%	68	1.056	41	49	45	9
50	75	4.9%	68	1.056	46	53	49.5	7
40	100	nd	53	1.042	18	24	21	14
40	80	5.6%	65	1.080	65	72	68.5	5
40	60	3.7%	81	1.131	457	Nd (*)	Nd (*)	Nd (*)
23	100	nd	53	1.101	90	120	105	14
23	80	5.6%	65	1.142	300	330	315	5
23	75	4.9%	68	1.152	492	515	503.5	2

(*)The sample stored at 40°C and 60%RH had not yet crystallized after 457 days. This point is not plotted on the following graphs since technically there was no t_m measured. but it is briefly mentioned in later discussion

(**) the uncertainty is taken as $(t_{nc} - t_c)/2\,t_{oc}$

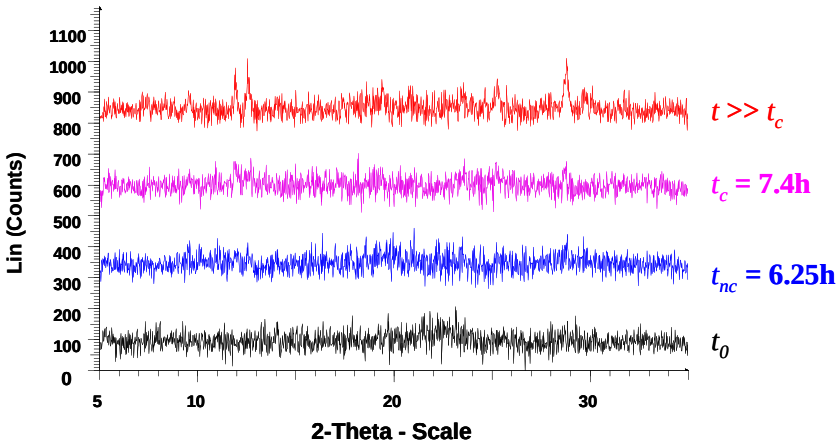

Fig. 7 XRPD diagrams of the solid dispersion SAR/HPMCP stored at 126°C and 0%RH at different times.

humidity and temperature of storage, can be described in terms of only one parameter, T_g/T, as was already observed by Miyazaki *et al.* (22) for the crystallization of nifedipine analogues; however in their study this was for $T > T_g$. The effect of the temperature rescaling is particularly dramatic for the observation of the point corresponding at 96°C, 0% RH (T_g/T=0.951). In Fig. 8 this point is well separated from the other sub-T_g points, whereas in the rescaled Fig. 9, it is well aligned with all other sub-T_g points.

- At $T > T_g$: there is a non Arrhenius behavior, which can correspond to the Adam-Gibbs-Vogel (AGV) model (see below), with much shorter crystallization times and a higher temperature dependence.

In the Appendix it is demonstrated by statistical means that there is no significant difference of behaviour for the three main humidity conditions: 75%RH, 80%RH and 100%RH.

DISCUSSION

Theoretical Interpretation

α–relaxations

In this section we propose an explanation of the observed results by the link between α-relaxations and crystallization.

The α-relaxations behave differently above and below the glass transition temperature, according to the Adam Gibbs model (6,14,32,33).

T >Tg

The molecular α-relaxation time τ_α is related to the temperature by the Vogel-Tammann-Fulcher (VTF) equation:

$$\tau_\alpha = \tau_{\alpha 0} \exp\left(\frac{D\, T_0}{T - T_0}\right) \tag{3}$$

where $\tau_{\alpha 0}$ is the limit for relaxation time at the high temperature limit, and T_0 is the temperature where τ becomes infinite. T_0 is often taken as the Kauzman temperature and D is a material specific parameter depending on the glass fragility. D is related to the fragility index m (defined in Eq. 4) by Eq. 5.

$$m = \left[\frac{d\log(\tau_\alpha(T))}{d(T_g/T)}\right]_{T=T_g} \tag{4}$$

$$D = \frac{2.303\, m_{\min}^2}{m - m_{\min}} \tag{5}$$

The minimum value of m, m_{min}, is close to 16, (34), thus:

$$m = m_{\min} + \frac{2.303\, m_{\min}^2}{D} \approx 16 + \frac{590}{D} \tag{6}$$

Table IV Crystallization Time Measurements for all the Samples Stored in Dessicators (at Controlled T and %RH) at T > T_g

Storage T (°C)	Storage RH (%)	T_g (°C)	T_g/T	t_{nc} (days)	t_c (days)	t_{oc} (days)	Uncertainty (%)
115	0	116	1.003	2.52	2.69	2.61	3
116	0	116	1.000	0.77	0.88	0.83	7
126	0	116	0.975	0.26	0.31	0.28	8
136	0	116	0.951	0.05	0.07	0.06	19

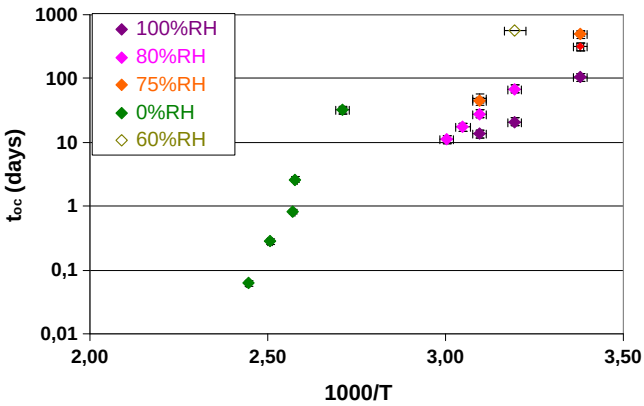

Fig. 8 Crystallization's onset as a function of 1000/*T*.

$$\frac{T_0}{T_g} = \left(1 - \frac{m_{\min}}{m}\right) \tag{7}$$

$T < T_g$

The glassy state below T_g is a non-equilibrium one (33), where the macroscopic configurational entropy remains constant and depends only on the fictive temperature T_f. As a consequence, τ_α has Arrhenius-like temperature dependence. The most common relation used to fit the temperature dependence to the relaxation times in this range is the so-called Adam-Gibbs-Vogel (AGV) equation (35):

$$\tau_\alpha = \tau_{\alpha 0} \exp\left(\frac{D\,T_0}{T\left(1 - T_0/T_f\right)}\right) \tag{8}$$

Pikal and co-workers (21) have shown that it is possible to fit experimental measurements of τ above and below T_g (measured by dielectric spectroscopy above T_g and by calorimetric method below T_g) using the same set of values for D and T_0.

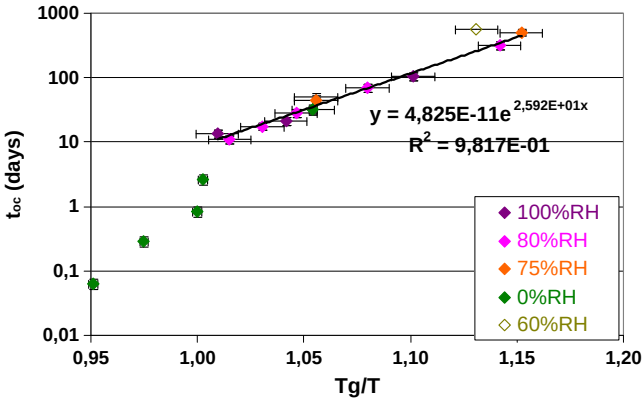

Fig. 9 Crystallization's onset as a function of T_g/T.

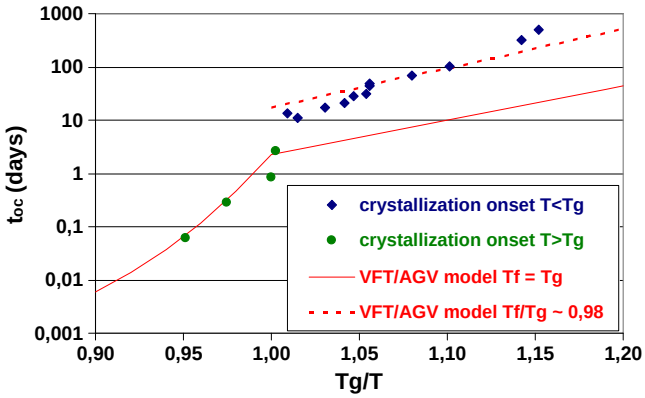

Fig. 10 Experimental data *versus* modified VTF/AGV equations.

Crystallization Onset: α–relaxations Relationship

As mentioned in the introduction, several studies (13,20) have related the chemical degradation or the crystallization rate in amorphous systems to the different relaxation times. In order to correlate the onset crystallization time (τ_{oc}) to the α relaxation time we propose to use an equation very close to that already proposed by Bughra *et al.* (13):

$$\log(\tau_{oc}) = \xi\ \log(\tau_\alpha) + \log(\tau_{oc}^0) \tag{9}$$

where $\xi \leq 1$ is a coupling parameter and τ_{oc}^0 is a constant.

When $T > T_g$, one expects therefore an apparent VTF law for crystallization time, as follows

$$\log(\tau_{oc}) = \log(\tau_{oc}^0) + \frac{1}{\ln(10)} \times \frac{D' T_0}{T - T_0} \tag{10}$$

By fitting experimental values of τ_{oc} one may obtain τ_{oc}^0, $D' = \xi D$ and T_0.

At $T < T_g$, the above equation may be modified according to AGV theory to:

$$\log(\tau_{oc}) = \log(\tau_{oc}^0) + \frac{1}{\ln(10)} \times \frac{\xi\, D\, T_0}{T\left(1 - T_0/T_f\right)} \tag{11}$$

Table V Fitting Parameters for the VTF Derived Equations (Eq. 8)

τ_{oc}^0	$7.95\ 10^{-7}$ days
T_0	324 K (T_g-T_0=65 K)
D'	2.99
m	96
D	7.4
ξ	0.40

Table VI VTF Parameters Values from Shamblin *et al.* 1999 (37)

	T_g (K)	T_0 (K)	T_g- T_0 (K)	D
Sorbitol	264	224	40	7.8
Sucrose	348	290	58	7.3
Trehalose	378	322	56	5.1
Indomethacin	322	256	66	8.9

Humidity Effect

When a hygroscopic amorphous solid is exposed to humidity, T_g usually rapidly decreases. However it has been shown that D is mostly independent of the moisture (27,36).

Therefore one can assume that, while T_0, T_g, T_f change will moisture uptake, the ratios T_0/T_g will remain constant, according to Eq. 7, and so will do the T_0/T_f since T_f and T_g are very close. The Eq. 11 can be so rewritten:

$$\ln(\tau_{oc}) = \ln(\tau_{oc}^0) + \frac{\xi\, D\, T_0/T_g}{(T/T_g) \times (1 - T_0/T_f)} \tag{12}$$

$$\ln(\tau_{oc}(T, RH)) = \log(\tau_{oc}^0) + A\, \frac{T_g(RH)}{T} \tag{13}$$

where $\boldsymbol{A}$ is a constant:

$$A = \frac{\xi\, D\, T_0/T_g}{(1 - T_0/T_f)} \tag{14}$$

Therefore the plot of τ_{oc} *versus* T_g/T is expected to be linear.

Comparison to the Experimental Results

In Fig. 10 we have superimposed the experimental results and the theoretical results according to the modified VFT/AGV equations.

At $T \geq T_g$ (0% RH)

The curve has been fitted to the experimental data by using the empirical equations quoted above (essentially the Eqs. 6 and 10). Best fit parameters (τ_{oc}°, T_0 *and* D') are given in Table V. Knowing that T_g at 0% RH was measured as 389 K (116°C), we can obtain: the fragility index m from the T_0/T_g ratio (Eq. 7), the D parameter from the VFT equation, and finally the ξ coupling exponent (Eq. 9). The m value obtained corresponds to that for a fragile glass. T_g-T_0 (= 65 K) and D values are in the range of values previously reported by Shamblin and collaborators (37) (cf Table VI). The ξ value is lower than those reported by Bhugra and Pikal (38) for pure products (0.75 for nifedipine and 1 for phenobarbital).

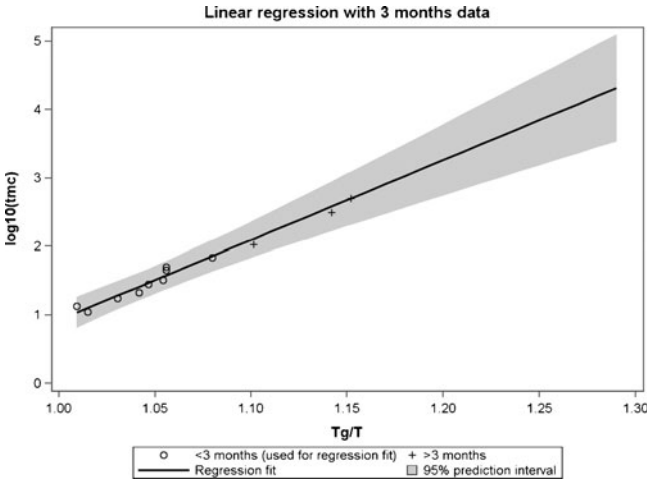

Fig. 11 Linear regression with 3 month data. * on this figure, the t_{oc} is noted as tmc, the mean crystallization time.

At $T \leq T_g$ (Various RH)

At $T < T_g$ we traced the theoretical onset of crystallization according to Eq. 11, by using the τ_{oc}°, T_0 and D' values obtained for the $T > T_g$ domain. Two hypotheses were evaluated:

- first a classical assumption that $T_f \sim T_g$ (corresponding to the full red line),
- secondly that T_f/T_g=0.98 whatever the moisture content (corresponding to the dotted red line). Note that T_f/T_g= 0.98 corresponds to $T_f = T_g$-8 K at 0% RH. This second point thus presumes that the actual product underwent some aging during its production process.

It is very clear from the plot that the crystallization times predicted for $T_f = T_g$ (no aging of the glass) are about one order of magnitude lower than the experimental data, even for T very close to T_g. In contrast, the prediction with $T_f/T_g \sim 0.98$ is much closer to the experimental data. In particular it explains a jump of the crystallization time between experiments just

Table VII Parameter Estimates With 3 Months Data

Label	DF	Parameter Estimate	StandardError	*t* Value	Pr > |t|	95% Confidence Limits	
Intercept	1	−10.75361	1.35152	−7.96	<.0001	−13.94946	−7.55777
Tg/T	1	11.68012	1.29538	9.02	<.0001	8.61703	14.74321

Table VIII Extrapolated mean crystallization time calculated from Eq. 14 and compared to experimental values

Storage T (°C)	Storage RH (%)	T_g/T	Experimental t_{oc} (days)	Predicted t_{oc} (days)	Calculated t_m (days) 95% lower limit	Calculated t_m (days) 95% upper limit	In the 95% prediction interval
23	100	1.101	105	130	83	199	Yes (−19%)
40	60	1.131	>570	287	150	555	No (> + 100%)
23	80	1.142	315	385	185	814	Yes (−16%)
23	75	1.152	504	506	224	1151	Yes (−0.4%)

above and just below T_g. However we may observe some deviation of the slope of the experimental correlation *versus* the theoretical line. This may be the consequence of a slight aging when the T_g/T values increase.

Finally, even if the theory - experiment agreement is not perfect, these data confirm that the presence of moisture leads to decreases in T_g, T_0, and T_f, while keeping mostly constant the T_g/T_0 and T_f/T_0 ratios. In addition, moisture does not change the fragility index *m*. The data also suggest that an experiment performed at $T > T_g$ cannot predict the crystallization behaviour at $T < T_g$, if one does not take into account the history of the glassy material (as expressed by T_f). Therefore one may expect a different crystallization rate for samples of the same composition obtained by a different process or even significantly different process conditions.

Long-Term Stability Prediction from 3 Month Data

In this section we examine the data corresponding to $T < T_g$ from an empirical and pragmatic point of view and determine if it is possible to predict the long term stability (up to 17 months) based on mid-term stability data (up to 3 month) according to rigorous statistical analysis (Table VII).

We fitted a linear model of Log 10(t_{oc}) *versus* T_g/T. From the fitted model with data of less than 3 months, the predicted mean response with a 95% predictive confidence interval is illustrated in Fig. 11. One can note that data above 3 months fall within the 95% prediction interval and are very close to the fit line.

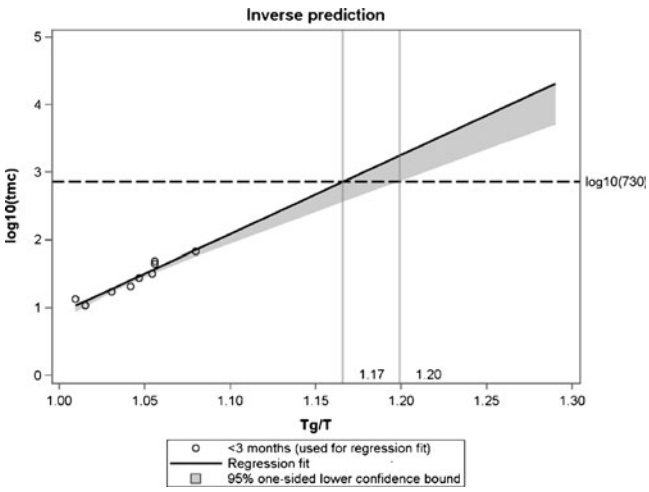

Fig. 12 Inverse prediction (model with the 3 months data).

In Table VIII, each one of the four experimental points is individually compared to the theoretical extrapolated values and to the limits of the 95% prediction interval. The experimental values are relatively close to the calculated ones, excepted for the point corresponding to the conditions 40°C and 60%RH. This point is not represented on the graphs since the sample had not yet crystallized after 17 months, but it would be outside the 95% prediction interval. This exceptional result might be an artefact or might be due to an unexplained phenomenon occurring during the storage. One hypothesis is that when an amorphous sample is stored for such a long time in such warm conditions, its real density increases significantly, and the molecular mobility is reduced.

Design Space

The prediction can also be used to design storage conditions from mid-term stability data. The inverse prediction, giving the T_g/T values from crystallization times (see Fig. 12), is presented in Table IX for some classical stability times (1 to 6 months; 1, 2 and 4 years). For example, the usual shelf life for pharmaceutical drugs is 2 years (730 days). The minimum T_g/T value to reach at least 730 days without crystallization should be more than 1.17 according to the regression line, or 1.20 when taking a safety margin at a 95% lower statistical limit.

Table IX Inverse Prediction at Different Days

Days	T_g/T (95% one-sided lower confidence bound)
30	1.05 (1.05)
90	1.09 (1.10)
180	1.11 (1.13)
365	1.14 (1.17)
730	1.17 (1.20)
1095	1.18 (1.22)

[a]Prediction at 730 and 1095 days are out of range. these results must be used/interpreted with caution

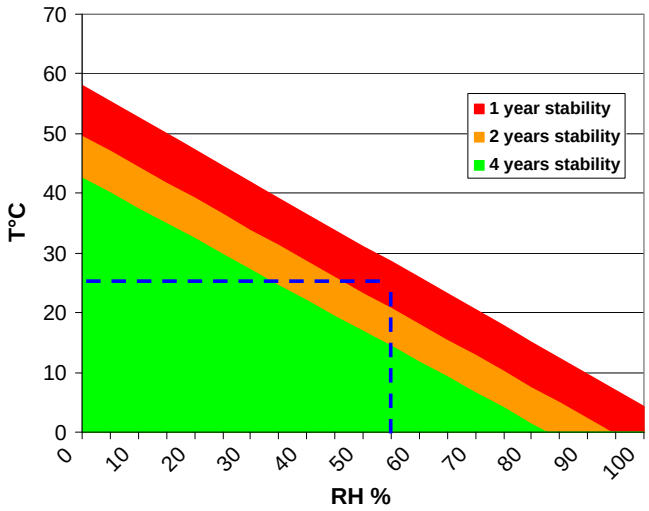

Fig. 13 The design space giving the storage conditions for different target shelf-lives.

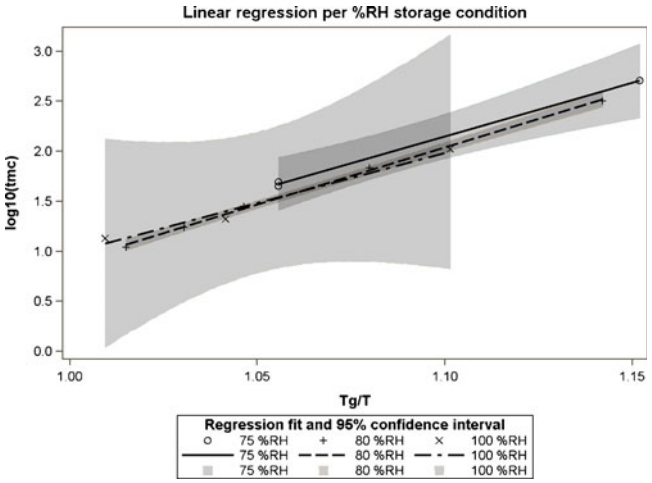

Fig. 14 Linear regression of the t_{mc} (or t_{oc}) as a function of T_g/T for different humidities (75, 80 and 100%RH).

By taking into account the correlation that was found between T_g and *RH*, a design space can be defined in the temperature and *RH* space for 1, 2 or 4 years. The design space presented in Fig. 13 is based on the lower statistical limit, by taking into account the safety margin. This graph predicts that, with a safety margin of 95%, this amorphous material could recrystallize between 1 and 2 years when stored at 25°C and 60% RH. It would therefore be necessary to store it under specific conditions, for example either 5°C or with desiccants at ambient temperature, in order to minimize any risk of crystallization. A 40°C temperature should be totally avoided.

CONCLUSION

In this study, crystallization times were measured for a pharmaceutical amorphous dispersion stored at different temperatures T below T_g, and different relative humidities. Results indicate that this crystallization time is correlated very simply to only one parameter, T_g/T. Moreover it is demonstrated that for $T < T_g$, the relation between the crystallization's onset and the rescaled inverse temperature T_g/T is an exponential law strictly independent of the *%RH*. This can be explained by noting that the moisture content does not change the D parameter, and therefore maintains a constant ratio of T_g/T_0. Below T_g, an effect of aging from the material's history is observed, meaning that the crystallization time is probably dependent on the material and the process to obtain it.

From a practical point of view, if the mid-term data (t_{oc} inferior to 3 months) are analyzed, and if the resulting exponential law is extrapolated to 18 months, it has been demonstrated that no significant discrepancy is observed between the calculated crystallization times and the measured ones. Consequently, this methodology can be used to design accelerated stability studies in order to anticipate physical destabilization for an amorphous drug product. The ultimate result of such an approach would be the definition of long term shelf life as early as possible in pharmaceutical development (even before phase 1 clinical studies), and the early design of appropriate packaging, adapted to the desired shelf life.

Finally, some restricted extensions of this methodology might be applicable for stability prediction. The extrapolation law, measured on a specific batch, might be extended to other batches as long as they are similar regarding certain properties. Indeed some physico-chemical characteristics seem to be very important for the kinetics of recrystallization. The residual solvent quantity can change the T_g of the drug product just like

Table X Table of ANCOVA: Type 3 Tests of Fixed Effects

Effect	Num DF	Den DF	*F* Value	Pr > F
H0: Equality of the slopes	2	5	1.54	0.3015
H'0: Equality of adjusted means	2	5	1.45	0.3181

H0: since $p > 0.25$. there is sufficient evidence to consider a common slope

H'0: since $p < 0.25$. there is sufficient evidence to consider a common intercept

water. The thermal history of the batches, as determined by the primary drying in the spray-drier and the secondary drying can anneal the amorphous powder and affect its molecular mobility. All such properties, which would potentially influence the drug product stability, could be identified as critical quality attributes of the amorphous intermediate drug product in a Quality by Design approach.

ACKNOWLEDGMENTS & DISCLOSURES

We acknowledge Marc-Antoine Perrin, Fabrice Tamagnan, Nancy Midoux, Cécile Bonvoisin, Lionel Gerbeau for their contribution to the SA project. We acknowledge Jean Alié, Jérome Menegotto, Marc Descamps, Rama Shmeis and Sophie-Dorothée Clas for their fruitful remarks and discussions.

APPENDIX: STATISTICAL CALCULATIONS

Data Pooling

The first question was: can we consider that the data obtained at 75, 80 and 100% RH is a unique population? A preliminary Analysis Of Covariance (ANCOVA) was conducted to test whether the data of the different %RH storage conditions could be pooled.

The table of ANCOVA (Table X) shows that the points (T_g/T, log 10(t_{mc})) for the different humidity conditions can be considered from a statistical point of view as the same population. The first important conclusion, is that the %RH impact should be taken into account only once in the calculation of T_g.

As illustration, we show the 3 different linear regressions for the different %RH on the same graph, see Fig. 14.

REFERENCES

1. Vasconcelos T, Sarmento B, Costa P. Solid dispersions as strategy to improve oral bioavailability of poor water soluble drugs. Drug Discov Today. 2007;12(23–24):1068–75.
2. Chiou WL, Riegelman S. Preparation and dissolution characteristics of several fast-release solid dispersions of Griseofulvin. J Pharm Sci. 1969;58(12):1505–10.
3. Simonelli AP, Mehta SC, Higughi WI. Dissolution rates of high energy PVP-sulfatiazole coprecipitates. J Pharm Sci. 1969;58(5):538–49.
4. Chowdary KPR, Babu KVVS. Dissolution, bioavailability and ulcerogenic studies on solid dispersions of Indomethacin in water soluble cellulose polymers. Drug Dev Ind Pharm. 1994;20:799–813.
5. Zerrouk N, Mennini N, Maestrelli F, Chemtob C, Mura P. Comparison of the effect of chitosan and polyvinylpyrrolidone on dissolution properties and analgesic effect of naproxen. Eur J Pharm Biopharm. 2004;57:93–9.
6. Hancock BC, Zografi G. Characteristics and significance of the amorphous state in pharmaceutical systems. J Pharm Sci. 1997;86:1–12.
7. Hancock BC, Parks M. What is the true solubility advantage for amorphous pharmaceuticals? Pharm Res. 2000;17(4):397–404.
8. Craig DQM, Royall PG, Kett VL, Hopton ML. The relevance of the amorphous state to pharmaceutical dosage forms: glassy drug and freeze dried systems. Int J Pharm. 1999;179:179–207.
9. Yu L. Amorphous pharmaceutical solids: preparation, characterization and stabilization. Adv Drug Deliv. 2001;48:27–42.
10. Leuner C, Dressman J. Improving drug solubility for oral delivery using solid dispersions. Eur J Pharm Sci. 2000;50:47–60.
11. Willart JF, Descamps M. Solid state amorphization of pharmaceuticals. Mol Pharm. 2008;5(6):905–20.
12. Yoshioka S, Aso Y. Correlations between molecular mobility and chemical stability during storage of amorphous pharmaceuticals. J Pharm Sci. 2007;96(5):960–80.
13. Bhugra C, Rambhatla S, Bakri A, Duddu SP, Miller DP, Pikal MJ, *et al.* Prediction of the onset of crystallization of amorphous sucrose below T_g from correlations with mobility. J Pharm Sci. 2007;96(5):1258–69.
14. Alie J, Menegotto J, Cardon P, Duplaa H, Caron A, Lacabanne C, *et al.* Dielectric study of the molecular mobility and the isothermal crystallization kinetics of an amorphous pharmaceutical drug substance. J Pharm Sci. 2004;93(1):218–33.
15. Konno H, Taylor LS. Influence of different polymers on the crystallization tendency of molecularly dispersed amorphous felodipine. J Pharm Sci. 2006;95(12):2692–705.
16. Serajuddin ATM. Solid Dispersion of poorly water-soluble drugs: early promises, subsequent problems, and recent breakthroughs. J Pharm Sci. 1999;88(10):1058–65.
17. Aso Y, Yoshioka S, Kojima S. Molecular mobility-based estimation of the crystallization rates of amorphous nifedipine and phenobarbital in PVP solid dispersions. J Pharm Sci. 2004;93(2):384–90.
18. Menegotto J, Alié J, Mayoux C, Bauer M. TSC and DDS. In: Zakrewski A, Zakrewski M, editors. Solid state characterization of pharmaceuticals; 2006.
19. Carpentier L, Decressain R, De Gusseme A, Neves C, Descamps M. Molecular mobility in glass forming fananserine: a dielectric, NMR, and TMDSC investigation. Pharm Res. 2006;23(4):798–805.
20. Aso Y, Yoshioka S, Kojima S. Explanation of the crystallization rate of amorphous nifedipine and phenobarbital from their molecular mobility as measured by 13C NMR time and the relaxation time obtained from the heating rate dependence of the T_g. J Pharm Sci. 2001;90(6):798–806.
21. Bhugra C, Shmeis R, Krill ST, Pikal MJ. Prediction of the Onset of Crystallization from experimental relaxation times I-correlation of molecular mobility from $T > T_g$ to $T < T_g$. Pharm Res. 2006;36(10):2277–90.
22. Miyazaki T, Yoshioka S, Aso Y, Kawanishi T. Crystallization rate of amorphous nifedipine analogues unrelated to the T_g. Int J Pharm. 2007;336:191–5.
23. Schmitt E, Davis CW, Long ST. Moisture-dependent crystallization of amorphous lamotrigine mesylate. J Pharm Sci. 1996;85(11):1215–9.
24. Andronis V, Zografi G. Crystal nucleation and growth of indomethacin polymorphs from the amorphous state. J Non-cryst Sol. 2000;271(3):236–48.
25. Zanotto ED, James PF. A theoretical and experimental assessment of systematic errors in nucleation experiments. J Non-cryst Sol. 1990;124(1):86–90.

26. Yang J, Grey K, Doney J. An improved kinetics approach to describe the physical stability of amorphous dispersions. Int J Pharm. 2010;384:24–31.
27. Yoshioka M, Hancock BC, Zografi G. Crystallization of indomethacin from the amorphous state below and above its glass transition temperature. J Pharm Sci. 1994;83(12):1700–5.
28. Khankari RK, Law D, Grant DJW. Determination of water content in pharmaceutical hydrates by differential scanning Calorimetry. Int J Pharmaceutics. 1992;82:117–21.
29. Tajber L, Corrigan OI, Healy AM. Physicochemical evaluation of PVP-thiazide diuretic interactions in co-spray-dried composites – analysis of glass transition composition relationships. Eur J Pharm Sci. 2005;24:553–63.
30. Nair R, Nyamweya N, Gönen S, Martinez-Miranda LJ, Hoag SW. Influence of various drugs on the glass transition temperature of PVP: a thermodynamic and spectroscopic investigation. Int J Pharm. 2001;225:83–96
31. Khougaz K, Clas S-D. Crystallization Inhibition in solid dispersions of MK-0591 and PVP polymers. J Pharm Sci. 2000;89(10):1325–34.
32. Angell CA. Formation of glasses from liquids and biopolymers. Science. 1995;267(5206):1924–35.
33. Hodge IM. Enthalpy relaxation and recovery in amorphous materials. J Non-cryst Sol. 1994;169(3):211–66.
34. Andronis V, Zografi G. The molecular mobility of supercooled amorhpous indomethacin as a function of temperature and RH. Pharm Res. 1998;15(6):835–42.
35. Hodge IM. Effects of annealing and prior history of enthalpy relaxation in glassy polymers. 6. Adams-Gibbs formulation of non-linearity. Macromolecules. 1987;20:2897–908.
36. Shalaev EY, Zografi G. How does residual water affect the solid-state degradation of drugs in the amorphous state. J Pharm Sci. 1996;85:1137–41.
37. Shamblin SL, Tang X, Chang L, Hancock BC, Pikal MJ. Characterization of the time scales of molecular motion in pharmaceutical important glasses. J Phys Chem B. 1999;103:4113–21.
38. Bhugra C, Pikal MJ. Role of Thermodynamic, molecular, and kinetic factors in crystallization from the amorphous state. J Pharm Sci. 2008;97(4):1329–49.